HHS Public Access

Author manuscript

Nat Neurosci. Author manuscript; available in PMC 2013 January 30.

Published in final edited form as:

Nat Neurosci. ; 15(2): 250–257. doi:10.1038/nn.3004.

Heterogeneous Reallocation of Presynaptic Efficacy in Recurrent Excitatory Circuits Adapting to Inactivity

Ananya Mitra[1], **Siddhartha S. Mitra**[2], and **Richard W. Tsien**[1]

[1]Department of Molecular and Cellular Physiology, Stanford University School of Medicine, Stanford, CA 94305, USA

[2]Institute of Stem Cell Biology and Regenerative Medicine Stanford University School of Medicine, Stanford, CA 94305, USA

Abstract

Recurrent excitatory circuits face extreme challenges in balancing efficacy and stability. We recorded from CA3 pyramidal neuron pairs in rat hippocampal slice cultures to characterize synaptic and circuit-level changes in recurrent synapses resulting from long-term inactivity. Chronic TTX-treatment greatly *reduced* the percentage of connected CA3-CA3 neurons but *enhanced* the strength of the remaining connections; presynaptic release probability sharply increased while quantal size was unaltered. Connectivity was decreased in activity-deprived circuits by functional silencing of synapses, whereas 3D anatomical analysis revealed no change in spine or bouton density or aggregate dendrite length. The silencing arose from enhanced Cdk5 activity and could be reverted by acute Cdk5 inhibition with roscovitine. Our results suggest that recurrent circuits adapt to chronic inactivity by reallocating presynaptic weights heterogeneously, strengthening certain connections while silencing others. This restricts synaptic output and input, preserving signaling efficacy among a subset of neuronal ensembles while also protecting network stability.

Keywords

homeostasis; adaptation; inactivity; recurrent circuits; morphology; connectivity

INTRODUCTION

Recurrent excitatory circuits are found throughout the brain[1], most prominently in computationally-intensive regions such as neocortex and hippocampal area CA3[2]. A single hippocampal CA3 neuron may use ~11,000 presynaptic boutons to recurrently excite other CA3 pyramidal cells[3]. This high intrinsic connectivity may support the operation of the CA3

Corresponding Author: Dr. Richard W. Tsien Department of Molecular and Cellular Physiology Stanford University School of Medicine 279 Campus Dr., Stanford, CA 94305 Phone (650) 725-7557 Fax (650) 725-8021 rwtsien@stanford.edu.

AUTHOR CONTRIBUTIONS: A.M. and R.W.T. designed the research and wrote the manuscript. A.M. and S.S.M. conducted the experiments. A.M. analyzed the data.

region in auto-associative memory processing[4] and pattern completion, a process wherein retrieval of a whole memory trace is triggered by activation of only a part of it[4–5]. Such operations engage clusters of strongly connected neurons[6–8] amongst a plethora of weaker connections, reflecting great heterogeneity in the likelihood and strength of individual connections.

All brain networks, be they recurrent or feed-forward, will encounter chronic variations in input levels during sleep[9], stroke and trauma[10], and neural degeneration. Synaptic homeostasis is a compensatory phenomenon, proposed to act like an overall gain control, enhancing synaptic weights when inputs are dampened and scaling them down when inputs are hyperactive[11]. Thus, neurons and networks would be kept away from extreme forms of activity, safeguarding neural information processing[11]. In some circumstances, homeostatic adaptation appears as a neuron-wide, postsynaptic scaling of excitatory postsynaptic currents due to varying abundance of postsynaptic glutamate receptors[11–13]. In other cases, adaptation can be local, synapse-specific and involve presynaptic alterations[14–19].

Differences in the modes of homeostasis engaged by recurrent and feed-forward networks would be expected because positive feedback loops in recurrent networks create a distinct potential for instability[20–21]. Indeed, clear disparities in responsiveness to chronic TTX-treatment have been found at feed-forward and recurrent excitatory synapses in hippocampus[22] and cortex[23]. In both regions, feed-forward projections undergo enhancement and recurrent connections display diminution of unitary synaptic responses. However, it remains unclear whether individual connections within the same topological class also display heterogeneity in adaptation. Network simulations predict that cell-wide synaptic scaling of recurrent synapses would generate striking instabilities[20]. However, the recurrent model circuit remains stable if individual synaptic weights are not yoked together by a single multiplicative factor, but endowed with greater autonomy[20]. Determining how excitatory synaptic weights may be adjusted to achieve a balance between network responsiveness and stability remains critical even as chronic inactivity causes alterations in intrinsic excitability[24–25] and network inhibition[23,26].

Homeostatic adaptation has often been approached by recordings of spontaneous miniature EPSCs (minis), which lump together inputs from all presynaptic partners of a particular class. This is advantageous for monitoring unitary synaptic events, but cannot provide direct information on network parameters such as the likelihood and strength of connections between single neurons. To overcome these restrictions, we used simultaneous paired recording technique in the CA3 region of organotypic rat hippocampal slices, isolating recurrent connections between individual pairs of neurons while keeping the excitatory and inhibitory projections to and from other areas of the slice intact. By obtaining an uncontaminated, high-resolution measurement of evoked excitatory transmission, we could address three key questions regarding homeostatic plasticity in recurrent circuits. Is the synaptic modification a homogeneous scaling across all synaptic connections of the same type? Does the synaptic modification arise from pre- or postsynaptic mechanisms? What kind of balance is struck between preservation of dynamic information transfer and avoidance of regenerative and runaway excitation? We found that that the recurrent CA3 hippocampal circuit displays multi-faceted adaptive mechanisms during chronic inactivity.

A combination of functional and morphological assays revealed changes in both the percentage of connected connectivity and synaptic strength of those pairs that remain in communication. Both have an underlying presynaptic basis and are regulated by cyclin-dependent kinase 5 (Cdk5), whose activation by interaction with p35/25 is dramatically enhanced by inactivity. Our experiments point to a striking reallocation of presynaptic efficacy in recurrent circuits that silences some connections while strengthening others, thus allowing net excitatory synaptic drive after chronic inactivity to remain similar to control levels. This arrangement may be essential to preserve information transfer, but also protecting network stability.

RESULTS

Activity deprivation decreased CA3 recurrent connectivity

We examined the functional properties of the associational connections between CA3 pyramidal neurons using simultaneous whole-cell recordings from pairs of neurons in organotypic rat hippocampal slices (Fig. 1). Organotypic slice cultures allow chronic (3–4 day) manipulations of slice conditions while maintaining an intact circuitry, largely similar to that found *in vivo*[27]. The recording of >200 individual pairs of potentially coupled CA3 neurons enabled us to compare the overall pattern of functional connectivity between excitatory neurons in chronically silenced (TTX-treated) versus control sister slices in a statistically meaningful way (Fig. 1). In synaptically connected cells (Fig. 1c, left), presynaptic action potentials (APs) elicited monosynaptic evoked excitatory postsynaptic currents (EPSCs) in the postsynaptic neuron. We considered a pair of neurons to be unconnected when there were no current responses time-locked to the presynaptic AP in >30 consecutive post-synaptic traces (Fig. 1c, right). We found the overall functional connectivity to be significantly *decreased*, from 45% in vehicle-treated control slices (N=90) to 20% in TTX-treated slices (N=131; $P<0.001$, χ^2-test; Fig. 1d). This decreased connectivity was not dependent on intersomatic distance (Fig. 1e). To minimize developmental changes that might confound the analysis of homeostatic adaptation, we studied mature slices between day *in vitro* (DIV) 21–28[27–28]. Within that time period, no significant differences were found between age groups DIV 21–24 and DIV 25–28 (Supplementary Fig. 1).

Synaptic strength increased between functionally coupled CA3 pairs—Fig. 2 focuses on CA3 pyramids that were functionally connected. Interestingly, we found that on average, actively connected neuron pairs in TTX-treated slices showed a dramatic 2.5–fold increase in synaptic strength (−26.8±3.8 pA control, N=41; −65.9±13.4 pA TTX-treated, N=26; P<0.005, *Kolmogorov-Smirnov* (*K-S*) test; Fig. 2b). A closer examination of the response kinetics at −60 mV revealed a ~3-fold faster rate of rise in the activity-deprived slices (10.5±1.6 pA/ms, control; 36.01±8.9 pA/ms, TTX-treated slices; $P<0.001$, *K-S* test; Fig. 2d) as well as a significant decrease in rise times (1.7±0.11 ms, control; 1.43±0.14 ms, TTX-treated slices; $P<0.05$, *K-S* test; Fig. 2e). The average latency of response was nearly identical in the two groups (2.3±0.16 ms, control; 2.3±0.21 ms, TTX-treated slices; Fig. 2f). Synaptic strength between the connected pairs was neither dependent on inter-somatic

distance (Fig. 2c) nor on the age of the slices during the recording period (Supplementary Fig. 2).

Given that we observed comparably-sized but opposite changes in connectivity and synaptic strength, we proceeded to compare the net excitatory drive per cell in control and chronically-silenced slices. We calculated the net recurrent excitatory drive per cell as

$$\sum_{t=1}^{N} (I_t/N)$$

where N is the total number of neuron pairs tested, I_i is the mean current of the i^{th} connection (including failures), and unconnected pairs contribute zero current. The net excitatory drive per cell was −1714.2 pA/130 = −13.2 pA in chronically silenced slices, very similar to the value in control slices (−1100.6 pA/90 = −12.2 pA). The lack of change was unexpected: the prevailing view of homeostatic adaptation to inactivity[29] would have predicted a net increase.

The adaptive changes in functional connectivity and synaptic efficacy were not due to alterations in the presynaptic AP parameters: both spike height and spike shape (half-width, spike area) were similar in control and TTX-treated slices (Supplementary Fig. 3). In addition, previous tests with small depolarizing current steps have shown similar intrinsic excitability of CA3 neurons under control and TTX-treated conditions[22].

Increased P_r contributes to heightened synaptic strength

The percentage of transmission failures between synaptically coupled neurons is inversely related to the release probability (P_r) and/ or the total number of functional synapses (N) between a pair. Activity-deprivation significantly reduced the number of transmission failures (32.5±8.6 %, control and 8.0±2.87 %, TTX-treated slices; $P<0.02$, *t*-test; Fig. 3a–b), indicating an increase in P_r and/or N.

To test for a relative change in P_r, we measured the ratio of EPSCs to a pair of APs at various time intervals ranging from 20–250 ms. Generally, synapses with high P_r show paired-pulse depression (EPSC2/EPSC1<1) whereas synapses with low P_r show paired-pulse facilitation (EPSC2/EPSC1>1). While control slices showed a slight paired pulse facilitation for the range of time intervals tested (EPSC2/EPSC1> 1), TTX-treated slices show significant paired pulse depression (EPSC2/EPSC1= 0.77) between time intervals 50–100 ms (Fig. 3c–d), consistent with an enhanced P_r. We subsequently focused on intervals of 50 ms to minimize possible errors arising from overlapping first and second responses at shorter intervals, as typical for studies of paired-pulse ratio (PPR). Linear regression analysis of PPR (50 ms) and EPSC1 size for individual pairs in control and TTX-treated conditions, revealed no significant correlation difference ($P>0.59$) between the individual groups (Supplementary Fig. 4); for the same initial synaptic strength, the level of PPR is similar in the two groups.

We also measured the response to 20 Hz trains of 5 APs and found a dramatic increase in short-term depression at activity-deprived recurrent synapses relative to the vehicle-treated slices (Fig. 3e–f).

Post-synaptic quantal size and synapse number remain unaltered

We used variance-mean (V-M) analysis to obtain a quantitative estimate of P_r as well as post-synaptic quantal size (q) and N between the pairs of functionally connected CA3 neurons. This method uses the theoretically expected parabolic relationship between the variance and mean of synaptic responses recorded under different release probability (paired pulse stimulation and/or different external calcium concentrations) to obtain estimates of P_r, q, and N(Fig. 4a–b)[30]. Dual-patch recording is ideally suited to address questions regarding quantal parameters of evoked responses by providing reliable and verifiable stimulation of a single presynaptic cell. We found a significant increase in P_r at recurrent synapses in activity-deprived slices compared to control (0.30±0.06 and 0.56±0.09 in control and TTX-treated slices, respectively; $P<0.03$, *t*-test) that corroborated findings from the paired-pulse experiments. But unlike classical homeostatic postsynaptic scaling of EPSC amplitude, $q_{control}$ and q_{TTX} did not appear to be different (−15.32±3.4 pA and −17.36±4.3 pA for control and TTX-treated slices, respectively; $P>0.66$; Fig. 4c), and were similar to the mEPSC amplitude at recurrent synapses reported previously[22]. The average values of N in control (10.3±3.5) and TTX-treated (15.6±5.3) slices were not significantly different ($P>0.41$; Fig. 4d).

Anatomical changes does not reflect decreased functional connectivity

In principle, morphological changes such as decreases in densities of spine or axonal varicosities or the total dendritic length could account for the decreased connectivity in the activity-deprived slices. Using *Neurolucida* (MBF bioscience), we reconstructed the three-dimensional morphology of EGFP-expressing CA3 pyramidal neurons in control and TTX-treated slices (Fig. 5a). The average spine density and axonal varicosity density were similar in control and TTX-treated slices, both in the *Strata oriens* and *radiatum* (Fig. 5e, f). We also examined dendritic branching and the aggregate length of the dendritic tree since this could in principle alter the extent of the postsynaptic target for neuron-neuron connectivity. No significant difference was seen in the number of apical branches (Fig. 5b, d right) or total length of dendrite (Fig. 5c). In contrast, we found a significant increase in branch number in the basal dendrites of the activity-deprived slices (Fig. 5c, d left). The increased branching took place away from the cell soma, at higher order branch points (branch order >6) rather than in primary or secondary branch points (Fig. 5d left). However, the total length of basal dendrites, which would determine the post-synaptic target size, was similar in neurons from control and TTX-treated slices (Fig. 5c). Given that the total dendritic length, spine density and axonal varicosity density were no different under activity-deprived conditions, the morphological evidence would suggest *similar* neuron-neuron connectivity, not the decreased functional connectivity directly observed with electrophysiological recordings.

Concerted vs. heterogeneous presynaptic effect on connectivity

An extreme scenario that could lead to the decreased connectivity that we observe in activity-deprived conditions involves a cell-wide alteration in presynaptic efficacy: some presynaptic CA3 neurons lose all connectivity with all of their downstream partners by a drastic presynaptic silencing at all their boutons, whereas other presynaptic CA3 neurons increase the strengths of all their connections. To test this possibility, we performed *triple* recording experiments in which we recorded from three neurons: a *single* presynaptic cell and, sequentially, *two* potential post-synaptic target cells (Supplementary Fig. 5). This allowed us to test the simplest and most extreme scenario, in which adaptation to inactivity leaves some presynaptic neurons perfectly connected to potential postsynaptic targets while others are not connected at all (Supplementary Fig. 5a). In such triple recording experiments (TTX-treated, N=4; control, N=5), we always found one of the post-synaptic partners to be connected while the other was not (Supplementary Fig. 5c), indicating that the presynaptic neuron had not lost all downstream connectivity. Thus, we can discount the possibility of an extreme presynaptic effect of either increased connection strength with all potential downstream partners or drastic presynaptic silencing at all boutons (Supplementary Fig. 5b).

Involvement of silent synapses in activity-deprived slices

One hypothesis to reconcile the lack of change in postsynaptic dendritic target size with the decreased functional connectivity invokes the conversion of a portion of active connections to functionally “silent” synapses. A reallocation of presynaptic resources has been found at the *Drosophila* neuromuscular junction, where Rab3 dynamically controls presynaptic release at individual active-zones[31]. We utilized four different strategies to see if unconnected pairs could be “awakened” and rendered functional. To test for presynaptically silent synapses, we used various approaches: we elevated extracellular Ca^{2+} from 2 mM to 3.7 mM (N=6, control; N=5, TTX-treated slices), and we stimulated presynaptic neurons to fire trains of 5 APs at 20 Hz (N=6, control; N=6, TTX-treated slices). In neither case were we able to detect AP-triggered responses in the postsynaptic cell.

As an additional test, we elevated cyclic adenosine monophosphate (cAMP) levels with forskolin, an adenylate cyclase activator. Enhancement of cAMP-dependent signaling has been shown to awaken presynaptically dormant synapses[32–33]. However, activating adenylate cyclase with 50 μM forskolin treatment (see Methods) did not alter the connectivity in activity-deprived slices (18%, N=11 and 19%, N=130 with and without forskolin, respectively; $P>0.5$ by χ^2-test) or in control slices (55%, N=11 and 45%, N=90, with and without forskolin, respectively; Fig. 6a–b; top- middle). There still remained a significant decrease in connectivity in TTX-treated slices compared to control slices even after forskolin treatment (55%, N=11, control with forskolin; 18%, N=11, TTX-treated with forskolin; $P<0.05$ by χ^2-test, Fig. 6a, middle).

Role of Cdk5 in presynaptic modification

We looked for possible involvement of another molecule, Cdk5, shown previously to be important for synaptic modulation on both sides of the synapse[34–37]. Cdk5 is regulated by chronic activity-deprivation in dissociated hippocampal cultures and enlarges the resting pool wherein vesicles are largely unavailable for evoked release[36]. By this mechanism, or

possibly others[37], Cdk5 potently inhibits neurotransmitter release, even producing presynaptic silencing at some nerve terminals[36]. To examine the role of Cdk5 in the activity-deprived recurrent synapses, we directly measured expression levels of Cdk5 protein from micro-dissected CA3 regions of control and TTX-treated organotypic slices. The two groups were not different in their total Cdk5 protein level (Fig. 6c). We went on to assess the association of Cdk5 with its regulatory activator p35 (or its constitutively active fragment p25), a hallmark of Cdk5 activation[38]. We first used co-immunoprecipitation (Co-IP) to assay for Cdk5 physically associated with p35 and p25, using anti-p35/25 antibody for immunoprecipitation of the complex followed by immuno-blotting with anti-Cdk5 antibody (see Methods). We found a ~6–fold increase in the level of Cdk5 protein bound to p35 and p25 in TTX-treated slices relative to control slices (control, n=42, N=4; TTX-treated, n=42, N=4; P<0.03, t-test; Fig. 6d). In the converse Co-IP assay, immunoprecipitation of the Cdk5-p35/p25 protein complex was performed with anti-Cdk5 antibody, followed by immuno-blotting with the anti- p35/25 antibody. This assay showed ~8–fold and ~6–fold increases in the respective levels of p35 and p25 protein bound to CDK5 in TTX-treated slices relative to control slices (control, n=42, N=4; TTX-treated, n=42, N=4; P<0.01, t-test; Fig. 6e). Total p35 and p25 protein levels were similar in control and chronically silenced slices (Supplementary Fig. 6).

Chronic inactivity can also result from long-term blockade of glutamate receptors. However, in tissue lysates of micro-dissected CA3 slices treated for 3–4 days with the AMPA receptor antagonist 2,3–dihydroxy–6–nitro–7–sulfamoyl–benzo[f]quinoxaline–2,3–dione (NBQX, 50 μM), we observed little change relative to control slices in the level of p35 and p25 protein bound to Cdk5 (data not shown). Thus, in this recurrent circuit, chronic AMPA receptor blockade appears to engage a different biochemical mechanism than chronic TTX-treatment (Fig. 6d–e, Supplementary Fig. 6).

Having found that the level of activated Cdk5 appears to be sharply increased in the TTX-treated slices, we next tested whether inhibition of Cdk5 might cause reversal of the functional silencing. Cdk5 was inhibited with roscovitine, a tri-substituted purine commonly used as a Cdk5 inhibitor[39]. Acute inhibition of Cdk5 with 50 μM roscovitine (with 30 min pre-incubation; see Methods) significantly elevated the connectivity of TTX-treated slices, increasing it from 20% (N=131, top) to 45% (N=31; P<0.001, χ^2-test; Fig. 6a, bottom). In the presence of the Cdk5 inhibitor, the level of connectivity was similar to the connectivity in control slices, either in the presence of roscovitine (47%, N=19, Fig. 6a, bottom) or in its absence (45%, N=90, Fig. 1 or Fig. 6a, top; P>0.5, χ^2-test). Thus, acute inhibition of Cdk5 caused the degree of synaptic connectivity to return to its basal level. Evidently, in TTX-treated slices, most of the basally connected pairs (~60% = (45%–19%)/45%) were silenced in a Cdk5-dependent manner.

Mindful of the striking increase in evoked EPSC size in activity-deprived slices, we examined the effect of Cdk5 inhibition on the strength of recurrent connections. In TTX-treated slices acutely exposed to roscovitine, the average strength of recurrent connections was −30.5±4.9 pA (N=17; Fig. 6b), much less than the connection strength in activity-deprived slices in the absence of Cdk5 inhibition (−65.9±13.4 pA, N=26; P<0.05, t-test), but not significantly different from connection strength in control slices, either in the presence

of roscovitine (−24.1±6.9 pA, N=6) or in its absence (−26.8±4.8 pA, N=41; $P>0.5$, *t*-test; Fig. 6b).

The lack of effect of roscovitine on control slices differs from prior studies showing that roscovitine enhances synaptic transmission in acute hippocampal slices[37]. One possible explanation is that the prior work focused on feed-forward, CA3 to CA1 synapses while our experiments were restricted to recurrent CA3 to CA3 synapses. The relevance of hippocampal area and/or circuit organization gains plausibility from previous findings showing differences in homeostatic adaptation in the same two hippocampal target regions[22].

Chronic activity-deprivation increased connection strength by a dramatic increase in P_r, evident from the significantly smaller PPR at 50 ms in TTX-treated slices (0.72±0.07) relative to control slices (1.15±0.11; $P<0.01$, *t*-test; Fig. 3b). The apparent difference in P_r between the control and TTX-treated slices was abolished by acute inhibition of Cdk5 (Supplemental Fig. 7). In the presence of roscovitine, PPR in activity-deprived slices (0.91±0.09, N=17) was not significantly different from control slices (0.96±0.16, N=6; $P>0.75$, *t*-test). Thus, Cdk5 inhibition caused the connection strength and PPR in TTX-treated slices to revert back to that of control slices.

The application of roscovitine to TTX-treated slices did not completely restore PPR to the same level as in control slices in the absence of drug (1.15±0.11). We interpret this in terms of an off-target effect of roscovitine in enhancing presynaptic Ca^{2+} channel activity[40] and thereby decreasing PPR. A hint of this effect is the trend towards decreased PPR even in control slices treated with roscovitine (0.96±0.16, drug versus 1.15±0.11, no drug). Any off-target, agonistic effect of roscovitine on Ca^{2+} channels is unlikely to account for the action of the drug on functional connectivity and connection strength, inasmuch as functional connectivity was unchanged by a sizeable elevation in the Ca^{2+}/Mg^{2+} ratio as previously mentioned. Likewise, an increase in synaptic strength by roscovitine would have weighed against the reversion of synaptic weight that was actually observed (Fig. 6b, bottom). Thus, we interpret the predominant effects of roscovitine in terms of Cdk5 inhibition. Our results not only point to the importance of CDK5 in supporting inactivity-induced changes in the recurrent circuit, but also suggest that the opposing effects on connectivity and presynaptic function may share some common mechanistic features.

DISCUSSION

We demonstrate that recurrent excitatory circuits undergo significant synaptic and circuit-level adaptive changes in response to chronic activity-deprivation in hippocampal area CA3. We found changes that were (1) highly non-uniform, (2) expressed presynaptically, (3) organized such that the net recurrent synaptic drive onto individual neurons remained unchanged, and (4) dependent on up-regulation of Cdk5 activity. These findings have important implications for information processing in recurrent excitatory circuits.

We show that adaptation is not uniform across all recurrent excitatory inputs on to a given CA3 neuron (see Fig. 7a–b). With chronic inactivity, functional associational connections

among CA3 neurons display a striking reduction in connectivity, become sparser by ~2.3–fold. At the same time, there is a dramatic ~2.5–fold increase in the efficacy of the remaining active connections. Having a heterogeneous (i.e. non-uniform) change such that the influence of a CA3 pyramidal neuron on its excitatory neighbors becomes concentrated over fewer postsynaptic cells but more potent on an individual basis – sparsifying and strengthening – allows the circuit to accentuate a select population of connections for greater signal-to-noise and to sustain the reliability of information processing[6–7,41].

One of the remarkable outcomes of our experiments is the extreme bifurcation in properties of connections in activity-deprived conditions. Given the high resolution of our recordings, a connection between a pair of neurons would be classified as functional even if only one vesicle were released at only one of the boutons on a single trial (out of >30 trials). The maximum P_r that that a single bouton could have and still masquerade as a silent synapse such that the CA3-CA3 pair appears unconnected, is very low (P_r<0.002; Supplementary Eq. 1), several orders of magnitude less than the P_r of boutons in connected pairs (see Fig. 4).

From the variance-mean analysis, the average number of synapses between a connected neuron pair was ~13. The decrease in connectivity requires that *all* the synapses between two previously coupled neurons be silenced. If the shut-down of individual synapses was stochastic, we would observe a graded spectrum of connection strengths and the likelihood of observing this extreme bifurcation of connectivity (where we see either unconnected or increased strength of remaining connections) would be very small (P<0.001, χ^2-test; Supplementary Eq. 2). Thus, for a CA3-CA3 pair to be assessed as non-connected, all of the individual synapses between that pair must be shut down in a cell-wide, all-or-none fashion. We speculate that the disconnection involves a functional coordination among presynaptic terminals onto the same postsynaptic cell and may engage a mechanism that is postsynaptically-initiated and retrogradely communicated at all synapses between the previously coupled pairs.

Our findings point strongly to a presynaptic mechanism for the strengthening at remaining connections. Assays of paired pulse, short-term plasticity, and variance-mean analysis indicated that the synaptic strengthening was due to significant increase in P_r but not in q or N. Moreover, utilization of a presynaptic mechanism as opposed to a postsynaptic mechanism offers several advantages. Computer simulations show that a presynaptic induction mechanism, in which the postsynaptic neurons preferentially potentiate synapses from presynaptic neurons that are more active, would allow a network to converge to a stable state[20]. In addition, *presynaptic* strengthening of connections would allow for information transfer for single or few APs but would offer protection from seizure-like activity due to the severe short-term depression associated with increased P_r (see ref.[22]).

Unlike classical homeostatic adaptation, which features a net increase in synaptic strength following activity-deprivation, the net effect of these countervailing changes was to produce a *similar* recurrent excitatory drive per cell pair in chronically silenced slices (−13.2 pA) as in control slices (−12.2 pA). Previous studies have suggested that chronic inactivity does not significantly alter the intrinsic excitability of CA3 neurons challenged with small steps of input current[22]. A combination of similar recurrent excitatory drive and unchanged intrinsic

excitability would allow spike-to-spike coupling to be maintained in the face of chronic inactivity.

Possible mechanism of Cdk5 in presynaptic modification

One of the critical findings of this study was that acute Cdk5 inhibition reversed chronic inactivity-driven changes in both connection probability and synaptic strength (Fig. 6, 7). The rescue was acute and essentially complete, and contrasted with the lack of effect of Cdk5 in non-silenced slices. This suggests that both effects are triggered by an inactivity-induced increase in the tonic Cdk5 activity, a conclusion confirmed by enhanced co-immunoprecipitation of Cdk5 with its endogenous activators p35 and p25 (Fig. 6d–e). The efficacy of Cdk5 inhibition in restoring connectivity sharply contrasted with the inability to awaken silent connections by well-established maneuvers aimed at increasing presynaptic function. Our findings have bearing on the locus of Cdk5 action in mediating the inactivity-dependent change in connectivity. Cdk5 is known to act postsynaptically to regulate dendritic spine retraction[42], but this is an unlikely mechanism in our studies, insofar as spine density in CA3 pyramidal neurons was very similar in control and TTX-treated slices (Fig. 6e). Presynaptically, Cdk5 could mediate silencing in various ways. A recent study suggests that enhancement of Cdk5 activity favors vesicle residency in the resting (largely unavailable) vesicle pool and leads to presynaptic silencing[36]. Thus, the strongly increased activation of Cdk5 we observed would be in line with functional silencing of nerve terminals. Alternatively, calcium channels and coupling between excitation and vesicle release may also be influenced by Cdk5 activation. Cdk5 has been shown to phosphorylate the II–III loop of P/Q-type calcium channels and to prevent the interaction of the channel with SNAP-25 and synaptotagmin, thus negatively regulating transmitter release[37].

While we found a significant increase in the association of Cdk5 with its activators p35/p25 in TTX-treated slices, total levels of Cdk5 and p35/p25 proteins were no different than control (Fig. 6, Supplementary Fig. 4). Thus, our results using tissue lysates from micro-dissected slices differed from data in TTX-treated dissociated hippocampal cultures where total Cdk5 level decreased[36]. This disparity likely arises from the different experimental systems. However, a common feature in both dissociated cultures[36] and organotypic slices (Fig. 6) is an inverse relationship between Cdk5 activity and presynaptic function.

Why are some synapses not silenced, but even stronger? Although the effects of Cdk5 on functional connectivity and synaptic strength might be mediated via separate and independent mechanisms, it is also possible that Cdk5 regulates both of these changes by a common mechanism. For example, in activity-deprived recurrent connections, Cdk5 activity might be spatially non-uniform, greatly concentrating at certain presynaptic terminals, thus silencing them, while being lowered in others, allowing their P_r to be enhanced. In this way, Cdk5 would directly implement the synaptic heterogeneity. Alternatively, active Cdk5 might be uniformly distributed, while the heterogeneity might arise from non-uniform activity of calcineurin (CaN), a phosphatase known to oppose actions of Cdk5[43]. Strong synapses would be maintained by a positive feedback loop involving Ca^{2+} entry, CaN activation, and basal openings of P/Q-type Ca^{2+} channels, while initially weak synapses would be driven to silence by the opposing action of Cdk5[37]. In this way, interplay between Cdk5 and CaN

(non-uniform) would lead to the synaptic heterogeneity. Finally, a heterogeneous allocation of synaptic weights could arise from competition/sharing of synaptic vesicles as previously found in invertebrate systems[31,44]. Constitutive bouton-to-bouton transport of vesicles occurs along mammalian axons[45]; in C. *elegans* axons, dynein-mediated retrograde transport of synaptic vesicle precursors falls under inhibitory control by Cdk5[46]. If similar control mechanisms operate in recurrent axons, Cdk5 activation would promote non-uniform deployment of synaptic vesicles resulting in sparser but stronger recurrent connections to specific postsynaptic targets.

Functional significance for network activity

Our studies on recurrent circuit properties were performed in cultured hippocampal slices which retain an intact circuitry largely similar to that found *in vivo*[27–28], but show enhanced connectivity as compared to acute slices of similar ages. Thus, the decrease in connectivity due to chronic silencing *in vitro* may not precisely reflect the amount of decrease *in vivo*. However qualitatively similar rules are likely to hold, based on published observations that while connectivity was greater in organotypic slices than *in vivo*, development after the first postnatal week continued at a remarkably similar rate in both preparations[28]. Thus, the finding of decreased connectivity but increased strength of remaining connections during chronic silencing may be important in offering qualitative insights into how recurrent circuits adapt to chronic inactivity.

The recurrent nature of CA3 circuit is important for auto-associative memory, particularly pattern completion[4]. Computer simulations show that an imbalance between connectivity and strength alters the effectiveness of pattern completion during memory storage and recall[47]. An example of such an imbalance is found in a mouse model of Down Syndrome (Ts65dn) which shows increased CA3 connectivity but a decrease in synaptic efficacy[48]. In behavioral studies, this mouse shows severe memory impairments[49]. On the other hand, we observe a decrease in connectivity but strengthening of select synapses in the TTX-treated slices. The overall outcome is maintenance of net excitatory drive per cell (control, −12.2 pA; TTX-treated, −13.2 pA). Given that the intrinsic excitability of CA3 neurons is also preserved[22], such changes would sharpen the completion of specific input patterns, with some patterns becoming more powerful at the expense of others. The overall outcome would be an improvement of network discrimination, but also protection against network instability[22].

Clinical conditions such as neuro-degeneration of afferent inputs, stroke, or trauma can result in chronic activity-deprivation and thus our study may be relevant to circuit changes in the aftermath of such conditions. The fact, that roscovitine completely rescues both connectivity and synaptic strength may have implications for its potential use as a therapeutic molecule for recovery of cognitive function. As a candidate anti-cancer drug (Seliciclib or CYC202), roscovitine has already successfully undergone PhaseI/IIa clinical trials[50]. This augurs well for the future development of roscovitine-like agents as potential therapeutic compounds for recovering recurrent circuit function after trauma or neural degeneration.

METHODS

Slice preparation

Hippocampal slices were prepared from Sprague-Dawley (Charles-River Laboratories, Wilmington, MA) rats at post-natal day 6 or 7. Hippocampi were dissected in ice-cold artificial cerebrospinal fluid (ACSF) consisting of (in mM) 122 NaCl, 3 KCl, 26 $NaHCO_3$, 1 NaH_2PO_4, 2 $CaCl_2$, 2 $MgCl_2$, 20 glucose (300–305 mOsm), bubbled with 95% O_2/5% CO_2. Four hundred micrometer thick slices were cut using a Stoelting Tissue Slicer (Stoelting Co.) followed by several washes with pre-warmed sterile culture medium. The slices were placed on culture membrane inserts (Millipore, Billerica, MA) at the interface of culture medium and air[27–28]. The medium was composed of 50% Hank's-based minimum essential media, 25% Hank's solution, 25% horse serum, 2 mM L-glutamine, 50 unit/mL penicillin, 50 μg/mL streptomycin and 10 mM HEPES, supplemented with 5 mM glucose (Invitrogen). Slices were kept at 37°C and medium was exchanged every 48–72 hours. All animal protocols were in compliance with the Institutional Animal Care and Use Committee of Stanford University.

Electrophysiology

Simultaneous whole-cell patch clamp recordings of the targeted pyramidal cells in area CA3 of hippocampal slice cultures (DIV 21–27) were obtained using two Multiclamp700B patch amplifiers (Molecular Devices, Union City, CA, USA), one in current-clamp mode (presynaptic cell) and the other in voltage clamp (postsynaptic neuron). All experiments were performed in oxygenated ACSF (bubbled with 95% O_2/5% CO_2) at room temperature. Results were not corrected for the liquid junction potential. Pyramidal cells in area CA3 were visualized by infrared differential interference contrast (DIC) microscopy. To chronically suppress neuronal activity, we treated slices with 1 μM TTX for 3–4 days, starting as early as 19 DIV. Slices were removed from TTX-containing media and washed with oxygenated ACSF for 10–15 min before commencing each recording. For activating adenylate cyclase, control and TTX-treated slices were treated with 50 μM Forskolin for 4 hrs at 37°C prior to recording. For inhibiting CDK5, control and TTX-treated slices were pre-incubated with 100 μM R-roscovitine 30 minutes at 37°C prior to recording and 50 μM roscovitine during the recording period. Glass electrodes (2–4 mΩ) were filled with an internal solution containing (in mM): 130 potassium gluconate, 7 KCl, 2NaCl (presynaptic cell) or cesium methyl sulphonate (postsynaptic cell), 10 Hepes, 1 $MgCl_2$, 2 mM ATP-Mg, 0.3 mM GTP-tris, 0.4 mM EGTA, 10 mM phosphocreatine, and 5 N–(2, 6–Dimethylphenylcarbamoylmethyl) triethylammonium chloride (QX314) (postsynaptic cell only), pH adjusted to 7.2 with KOH or CsOH. Presynaptic neurons were held in standard `current clamp' mode and postsynaptic neurons were held in voltage clamp mode using a MultiClamp700B (Molecular Devices, Union City, CA, USA). Presynaptic cells were kept at approximately −70 mV by injection of a bias current and APs were generated by 5 ms current pulses (typically 100 pA) and were elicited at 0.1 Hz throughout the duration of each paired recording. Evoked monosynaptic excitatory postsynaptic currents (EPSCs) were recorded in voltage-clamp (V-clamp) configuration held at −60 mV in response to presynaptic AP firing. We chose −60 mV as the holding potential for the postsynaptic cell since the reversal potential for chloride was ~ −60mV under our recording conditions. This

allowed the isolation of monosynaptic EPSCs without contaminating di-synaptic inhibitory post-synaptic current (IPSC). Series resistance (*<20 MΩ*) was monitored in all recordings of synaptic currents and recordings were terminated if changes in resistance >15% occurred. Experiments used in variance-mean analysis were carried out in ACSF containing 2.0mM Ca^{+2} (normal) and either 1mM Ca^{+2}(low) and/or 3.7mM Ca^{+2}(high). The Mg^{+2} concentration was adjusted to keep the total divalent ion concentration equal to 4mM in each case. For every experimental condition, data from TTX-treated slices were compared with those from vehicle-treated control slices.

Morphology

Individual CA3 neurons were electroporated with DNA (1–2 μg/μL) encoding EGFP at DIV 14–18. These slices were fixed (4% paraformaldehyde) at DIV 24–25, stained using standard immuno-staining techniques, and visualized using a LSM510 Meta Confocal Microscope and a 63× oil-immersion objective (Zeiss, NA: 1.4). The basal and apical dendrites of well-stained neurons were reconstructed in three dimensions using a Neurolucida system (Microbrightfield, Williston, VT). No correction was made for tissue shrinkage.

Drugs

All drugs were obtained from Tocris (Ellisville, MO, USA) and used in the following concentrations (μM): 1 tetrodotoxin (TTX), 50 forskolin, and 10 NBQX. R-roscovitine (EMD Chemicals, San Diego, CA, USA) was used at 50 μM during recording and 100 μM for the 30 minute pre-incubation.

Data analysis

All electrophysiology data acquisition and analysis was carried out using *pClamp9* (Molecular Devices) software, while Neuroexplorer (Microbrightfield, Williston, VT) was used for morphometric analysis. Results are expressed as means and standard errors. The physiological and morphological properties between TTX-treated and vehicle treated control groups were compared using either an unpaired, two-tailed *Student t*-test for normalized data sets or *Kolmogrov-Smirnov* (*K-S*) test for data sets that were not normally distributed (unless otherwise noted). The probability of connection was assessed using a two-tailed Pearson's chi-square (χ^2 test.

Western blot analysis and immunoprecipitation

CA3 region of organotypic hippocampal slices DIV 21–25 were micro-dissected under a stereomicroscope and homogenized in lysis buffer (20 mM Tris, pH 7.6, 150 mM NaCl and 1 mM EDTA) with protease and phosphatase inhibitors (Roche Applied Science, Indianapolis, IN, USA). To assay total levels of Cdk5, p35, p25 and Tuj1 protein, 20 μg of protein was separated on 12% SDS-PAGE gels and transferred to nitrocellulose membrane. The following antibodies were used anti-Cdk5 (mouse monoclonal: clone DC17, Millipore, Billerica, MA), anti-p35/p25 (Rabbit monoclonal: clone C64B10, Cell Signaling Technology, Danvers, MA) and anti-Tubulin, Beta III isoform (Tuj1; mouse monoclonal: clone TU-20, Millipore, Billerica, MA). The protein of interest was detected and quantitated

using the infrared (LI-COR Odyssey) fluorescent detection system. Cdk5 levels were normalized to their respective Tuj1 levels. For immunoprecipitation, 500 μg of protein was immunoprecipitated using sepharose beads and eluted using 4× SDS-PAGE loading buffer. For each group (control and TTX-treated), a total of 42 slices (n) were analyzed from 4 different organotypic culture batches (N).

Supplementary Material

Refer to Web version on PubMed Central for supplementary material.

ACKNOWLEDGMENTS

We thank Drs. M. Pathak, V. Dhani, and S. Owen for comments on the manuscript, I. Prada for advice on immunostaining techniques, and R.W.T. laboratory members for helpful discussions throughout the project. This work was supported by National Institute of Mental Health grant 5R37MH071739 to R.W.T.

REFERENCES

1. Silberberg G, Grillner S, LeBeau FE, Maex R, Markram H. Synaptic pathways in neural microcircuits. Trends Neurosci. 2005; 28:541–551. doi:S0166-2236(05)00212-2 [pii] 10.1016/j.tins.2005.08.004. [PubMed: 16122815]
2. Buzsaki, G. Oxford University Press; USA: 2006. p. 464
3. Wittner L, Henze DA, Zaborszky L, Buzsaki G. Three-dimensional reconstruction of the axon arbor of a CA3 pyramidal cell recorded and filled in vivo. Brain Struct Funct. 2007; 212:75–83. doi:10.1007/s00429-007-0148-y. [PubMed: 17717699]
4. Guzowski JF, Knierim JJ, Moser EI. Ensemble dynamics of hippocampal regions CA3 and CA1. Neuron. 2004; 44:581–584. doi:S0896627304007172 [pii] 10.1016/j.neuron.2004.11.003. [PubMed: 15541306]
5. Rolls ET, Kesner RP. A computational theory of hippocampal function, and empirical tests of the theory. Prog Neurobiol. 2006; 79:1–48. doi:S0301-0082(06)00036-0 [pii] 10.1016/j.pneurobio.2006.04.005. [PubMed: 16781044]
6. Song S, Sjostrom PJ, Reigl M, Nelson S, Chklovskii DB. Highly nonrandom features of synaptic connectivity in local cortical circuits. PLoS Biol. 2005; 3:e68. doi:04-PLBI-RA-0489R2 [pii] 10.1371/journal.pbio.0030068. [PubMed: 15737062]
7. Lefort S, Tomm C, Floyd Sarria JC, Petersen CC. The excitatory neuronal network of the C2 barrel column in mouse primary somatosensory cortex. Neuron. 2009; 61:301–316. doi:S0896-6273(08)01092-1 [pii] 10.1016/j.neuron.2008.12.020. [PubMed: 19186171]
8. Hardingham NR, et al. Quantal analysis reveals a functional correlation between presynaptic and postsynaptic efficacy in excitatory connections from rat neocortex. J Neurosci. 2010; 30:1441–1451. doi:30/4/1441 [pii] 10.1523/JNEUROSCI.3244-09.2010. [PubMed: 20107071]
9. Bushey D, Tononi G, Cirelli C. Sleep and synaptic homeostasis: structural evidence in Drosophila. Science. 2011; 332:1576–1581. doi:332/6037/1576 [pii] 10.1126/science.1202839. [PubMed: 21700878]
10. Butz M, van Ooyen A, Worgotter F. A model for cortical rewiring following deafferentation and focal stroke. Front Comput Neurosci. 2009; 3:10. doi:10.3389/neuro.10.010.2009. [PubMed: 19680468]
11. Turrigiano GG, Leslie KR, Desai NS, Rutherford LC, Nelson SB. Activity-dependent scaling of quantal amplitude in neocortical neurons. Nature. 1998; 391:892–896. doi:10.1038/36103. [PubMed: 9495341]
12. O'Brien RJ, et al. Activity-dependent modulation of synaptic AMPA receptor accumulation. Neuron. 1998; 21:1067–1078. doi:S0896-6273(00)80624-8 [pii]. [PubMed: 9856462]

13. Aoki C, et al. Drebrin a knockout eliminates the rapid form of homeostatic synaptic plasticity at excitatory synapses of intact adult cerebral cortex. J Comp Neurol. 2009; 517:105–121. doi: 10.1002/cne.22137. [PubMed: 19711416]
14. Bacci A, et al. Chronic blockade of glutamate receptors enhances presynaptic release and downregulates the interaction between synaptophysin-synaptobrevin-vesicle-associated membrane protein 2. J Neurosci. 2001; 21:6588–6596. doi:21/17/6588 [pii]. [PubMed: 11517248]
15. Burrone J, O'Byrne M, Murthy VN. Multiple forms of synaptic plasticity triggered by selective suppression of activity in individual neurons. Nature. 2002; 420:414–418. doi:10.1038/nature01242 nature01242 [pii]. [PubMed: 12459783]
16. Thiagarajan TC, Lindskog M, Tsien RW. Adaptation to synaptic inactivity in hippocampal neurons. Neuron. 2005; 47:725–737. doi:S0896-6273(05)00647-1 [pii] 10.1016/j.neuron.2005.06.037. [PubMed: 16129401]
17. Lindskog M, et al. Postsynaptic GluA1 enables acute retrograde enhancement of presynaptic function to coordinate adaptation to synaptic inactivity. Proc Natl Acad Sci U S A. 2010; 107:21806–21811. doi:1016399107 [pii] 10.1073/pnas.1016399107. [PubMed: 21098665]
18. Jakawich SK, et al. Local presynaptic activity gates homeostatic changes in presynaptic function driven by dendritic BDNF synthesis. Neuron. 2010; 68:1143–1158. doi:S0896-6273(10)00976-1 [pii] 10.1016/j.neuron.2010.11.034. [PubMed: 21172615]
19. Beique JC, Na Y, Kuhl D, Worley PF, Huganir RL. Arc-dependent synapse-specific homeostatic plasticity. Proc Natl Acad Sci U S A. 2011; 108:816–821. doi:1017914108 [pii] 10.1073/pnas.1017914108. [PubMed: 21187403]
20. Buonomano DV. A learning rule for the emergence of stable dynamics and timing in recurrent networks. J Neurophysiol. 2005; 94:2275–2283. doi:94/4/2275 [pii] 10.1152/jn.01250.2004. [PubMed: 16160088]
21. Houweling AR, Bazhenov M, Timofeev I, Steriade M, Sejnowski TJ. Homeostatic synaptic plasticity can explain post-traumatic epileptogenesis in chronically isolated neocortex. Cereb Cortex. 2005; 15:834–845. doi:bhh184 [pii] 10.1093/cercor/bhh184. [PubMed: 15483049]
22. Kim J, Tsien RW. Synapse-specific adaptations to inactivity in hippocampal circuits achieve homeostatic gain control while dampening network reverberation. Neuron. 2008; 58:925–937. doi:S0896-6273(08)00418-2 [pii] 10.1016/j.neuron.2008.05.009. [PubMed: 18579082]
23. Maffei A, Turrigiano GG. Multiple modes of network homeostasis in visual cortical layer 2/3. J Neurosci. 2008; 28:4377–4384. doi:28/17/4377 [pii] 10.1523/JNEUROSCI.5298-07.2008. [PubMed: 18434516]
24. Desai NS, Rutherford LC, Turrigiano GG. Plasticity in the intrinsic excitability of cortical pyramidal neurons. Nat Neurosci. 1999; 2:515–520. doi:10.1038/9165. [PubMed: 10448215]
25. Trasande CA, Ramirez JM. Activity deprivation leads to seizures in hippocampal slice cultures: is epilepsy the consequence of homeostatic plasticity? J Clin Neurophysiol. 2007; 24:154–164. doi: 10.1097/WNP.0b013e318033787f 00004691-200704000-00009 [pii]. [PubMed: 17414971]
26. Maffei A, Nataraj K, Nelson SB, Turrigiano GG. Potentiation of cortical inhibition by visual deprivation. Nature. 2006; 443:81–84. doi:nature05079 [pii] 10.1038/nature05079. [PubMed: 16929304]
27. Muller D, Buchs PA, Stoppini L. Time course of synaptic development in hippocampal organotypic cultures. Brain Res Dev Brain Res. 1993; 71:93–100. [PubMed: 8432004]
28. De Simoni A, Griesinger CB, Edwards FA. Development of rat CA1 neurones in acute versus organotypic slices: role of experience in synaptic morphology and activity. J Physiol. 2003; 550:135–147. doi:jphysiol.2003.039099 [pii] 10.1113/jphysiol.2003.039099. [PubMed: 12879864]
29. Turrigiano GG, Nelson SB. Hebb and homeostasis in neuronal plasticity. Curr Opin Neurobiol. 2000; 10:358–364. doi:S0959-4388(00)00091-X [pii]. [PubMed: 10851171]
30. Saviane C, Silver RA. Estimation of quantal parameters with multiple-probability fluctuation analysis. Methods Mol Biol. 2007; 403:303–317. doi:10.1007/978-1-59745-529-9_19. [PubMed: 18828002]
31. Graf ER, Daniels RW, Burgess RW, Schwarz TL, DiAntonio A. Rab3 dynamically controls protein composition at active zones. Neuron. 2009; 64:663–677. doi:S0896-6273(09)00884-8 [pii] 10.1016/j.neuron.2009.11.002. [PubMed: 20005823]

32. Moulder KL, et al. A specific role for Ca2+-dependent adenylyl cyclases in recovery from adaptive presynaptic silencing. J Neurosci. 2008; 28:5159–5168. doi:28/20/5159 [pii] 10.1523/JNEUROSCI.5317-07.2008. [PubMed: 18480272]
33. Ma L, Zablow L, Kandel ER, Siegelbaum SA. Cyclic AMP induces functional presynaptic boutons in hippocampal CA3-CA1 neuronal cultures. Nat Neurosci. 1999; 2:24–30. doi:10.1038/4525. [PubMed: 10195176]
34. Su SC, Tsai LH. Cyclin-Dependent Kinases in Brain Development and Disease. Annu Rev Cell Dev Biol. 2010 doi:10.1146/annurev-cellbio-092910-154023.
35. Lai KO, Ip NY. Recent advances in understanding the roles of Cdk5 in synaptic plasticity. Biochim Biophys Acta. 2009; 1792:741–745. doi:S0925-4439(09)00094-5 [pii] 10.1016/j.bbadis.2009.05.001. [PubMed: 19442718]
36. Kim SH, Ryan TA. CDK5 serves as a major control point in neurotransmitter release. Neuron. 2010; 67:797–809. doi:S0896-6273(10)00613-6 [pii] 10.1016/j.neuron.2010.08.003. [PubMed: 20826311]
37. Tomizawa K, et al. Cdk5/p35 regulates neurotransmitter release through phosphorylation and downregulation of P/Q-type voltage-dependent calcium channel activity. J Neurosci. 2002; 22:2590–2597. doi:20026252 22/7/2590 [pii]. [PubMed: 11923424]
38. Tsai LH, Delalle I, Caviness VS Jr. Chae T, Harlow E. p35 is a neural-specific regulatory subunit of cyclin-dependent kinase 5. Nature. 1994; 371:419–423. doi:10.1038/371419a0. [PubMed: 8090221]
39. Meijer L, et al. Biochemical and cellular effects of roscovitine, a potent and selective inhibitor of the cyclin-dependent kinases cdc2, cdk2 and cdk5. Eur J Biochem. 1997; 243:527–536. [PubMed: 9030781]
40. Yan Z, Chi P, Bibb JA, Ryan TA, Greengard P. Roscovitine: a novel regulator of P/Q-type calcium channels and transmitter release in central neurons. J Physiol. 2002; 540:761–770. doi:PHY_13376 [pii]. [PubMed: 11986366]
41. Tao L, Cai D, McLaughlin DW, Shelley MJ, Shapley R. Orientation selectivity in visual cortex by fluctuation-controlled criticality. Proc Natl Acad Sci U S A. 2006; 103:12911–12916. doi:0605415103 [pii] 10.1073/pnas.0605415103. [PubMed: 16905648]
42. Fu WY, et al. Cdk5 regulates EphA4-mediated dendritic spine retraction through an ephexin1-dependent mechanism. Nat Neurosci. 2007; 10:67–76. doi:nn1811 [pii] 10.1038/nn1811. [PubMed: 17143272]
43. Tan TC, et al. Cdk5 is essential for synaptic vesicle endocytosis. Nat Cell Biol. 2003; 5:701–710. doi:10.1038/ncb1020 ncb1020 [pii]. [PubMed: 12855954]
44. Park M, et al. CYY-1/Cyclin Y and CDK-5 Differentially Regulate Synapse Elimination and Formation for Rewiring Neural Circuits. Neuron. 2011; 70:742–757. doi:S0896-6273(11)00303-5 [pii] 10.1016/j.neuron.2011.04.002. [PubMed: 21609829]
45. Darcy KJ, Staras K, Collinson LM, Goda Y. Constitutive sharing of recycling synaptic vesicles between presynaptic boutons. Nat Neurosci. 2006; 9:315–321. doi:nn1640 [pii] 10.1038/nn1640. [PubMed: 16462738]
46. Ou CY, et al. Two cyclin-dependent kinase pathways are essential for polarized trafficking of presynaptic components. Cell. 2010; 141:846–858. doi:S0092-8674(10)00385-5 [pii] 10.1016/j.cell.2010.04.011. [PubMed: 20510931]
47. Hanson JE, Madison DV. Imbalanced pattern completion vs. separation in cognitive disease: network simulations of synaptic pathologies predict a personalized therapeutics strategy. BMC Neurosci. 2010; 11:96. doi:1471-2202-11-96 [pii] 10.1186/1471-2202-11-96. [PubMed: 20704756]
48. Hanson JE, Blank M, Valenzuela RA, Garner CC, Madison DV. The functional nature of synaptic circuitry is altered in area CA3 of the hippocampus in a mouse model of Down's syndrome. J Physiol. 2007; 579:53–67. doi:jphysiol.2006.114868 [pii] 10.1113/jphysiol.2006.114868. [PubMed: 17158177]
49. Costa AC, Stasko MR, Schmidt C, Davisson MT. Behavioral validation of the Ts65Dn mouse model for Down syndrome of a genetic background free of the retinal degeneration mutation

Pde6b(rd1). Behav Brain Res. 2010; 206:52–62. doi:S0166-4328(09)00512-9 [pii] 10.1016/j.bbr.2009.08.034. [PubMed: 19720087]

50. Krystof V, Uldrijan S. Cyclin-dependent kinase inhibitors as anticancer drugs. Curr Drug Targets. 2010; 11:291–302. doi:CDT-Azevedo HT-3 [pii]. [PubMed: 20210754]

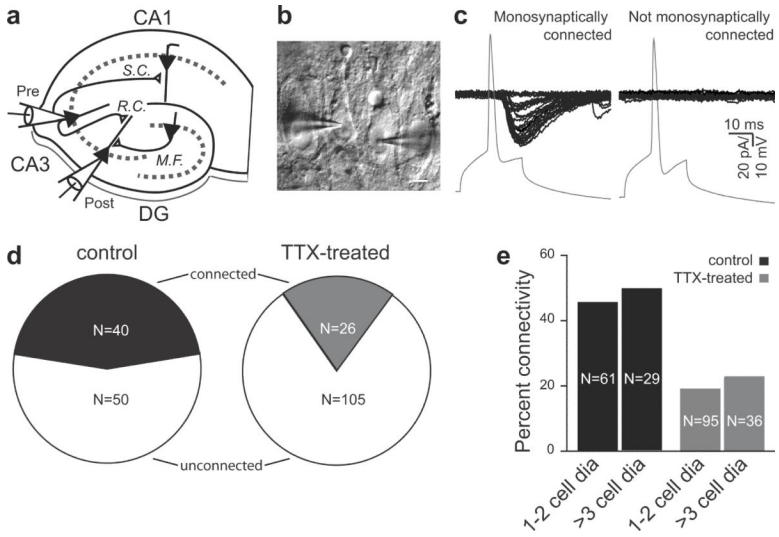

Figure 1. Adaptation of recurrent CA3 connections following chronic TTX-treatment

(**a**) Schematic of the excitatory hippocampal circuit with a paired-patch recording configuration in the CA3 region. CA3 pyramidal cells receive mossy fiber (M.F.) inputs from the dentate gyrus (DG) granule cells as well as recurrent collaterals (R.C.) from neighboring CA3 pyramidal cells. The Schaffer collaterals (S.C.) are the output of CA3 pyramidal neurons onto CA1 pyramidal neurons.

(**b**) Example IR-DIC image of a paired-recording from two CA3 neurons that were connected. Scale bar represents 10 μm.

(**c**) Example paired-recordings from a mono-synaptically coupled (left) and synaptically unconnected (right) pair of CA3 neurons. APs (gray, bottom trace) were generated with brief depolarizing current injections in the presynaptic neuron under I-clamp. The resulting evoked excitatory currents (EPSCs) were recorded in the postsynaptic neuron in V-clamp as it allowed the isolation of monosynaptic EPSCs without contaminating di-synaptic inhibitory postsynaptic current when the postsynaptic neuron was held at the reversal potential for chloride (~ −60 mV under our recording conditions).

(**d**) Percentage of connected CA3 pyramids in control (black, N=90) and TTX-treated (gray, N=131) slices. Percentages of unconnected pairs in each group are represented in white.

(**e**) The connectivity in control (black) and TTX-treated (gray) slices was ~45% and ~20% respectively, whether cell bodies of the neuron pairs were adjacent to one another or ≥3 cell bodies away (P >0.5; χ^2-test for both groups in control and TTX-treated slices).

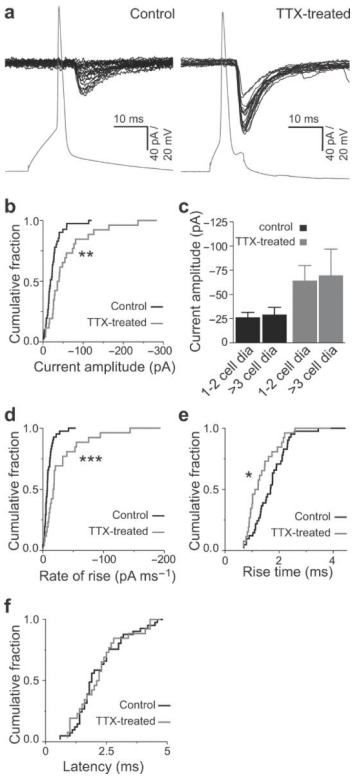

Figure 2. Synaptic efficacy of mono-synaptically connected CA3 pyramids following chronic inactivity

(**a**) Example simultaneous recordings from a synaptically coupled pair of CA3 neurons in control (left) and TTX-treated (right) slices.

(**b**) Cumulative plot of average synaptic strength of individual connected pairs in control (black) and TTX-treated (gray) slices. For each connected pair, the average amplitude of the EPSC was calculated from at least 30 trials, including measurements of zero amplitude when synaptic transmission failed. The average EPSC amplitude in TTX-treated recurrent connections (N=26) was significantly larger than in control connections (N=41; ***P* <0.005, *K-S* test).

(**c**) Synaptic strength (EPSC amplitude) as function of inter somatic distance between the preand postsynaptic CA3 pyramids in control (black) and TTX-treated (gray) slices. Error bars represent s.e.m.

(**d–f**) Cumulative plot showing a significant increase in the average EPSC rise times (**d**) and rate of rise (**e**) of individual connected pairs in chronically silenced slices but no change in response latency (**f**). Control (black) and TTX-treated (gray) slices (**P* <0.05, ****P* <0.001, *K-S* test).

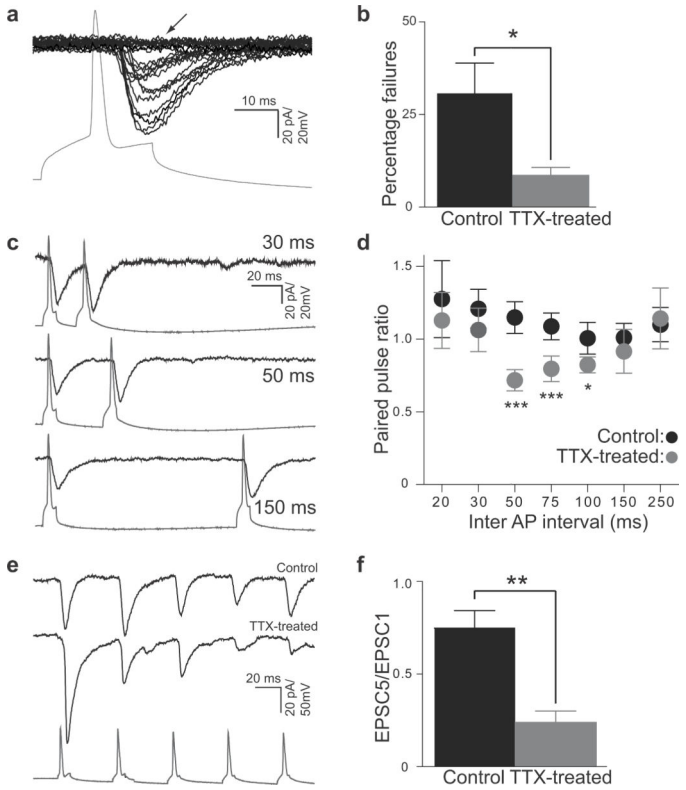

Figure 3. Chronic silencing leads to alterations in P_r between synaptically connected CA3 neurons

(**a**) Example traces from a connected CA3 pair with synaptic transmission failures (arrow). The incidence of failures (zero amplitude events) was determined for synaptically connected neurons from at least 100 consecutive trials.

(**b**) Average percentage of failures was significantly decreased in connected CA3 pairs from activity-deprived slices (control, black, N=13; TTX-treated, gray, N=12; P <0.05, *K-S* test).

(**c**) Example traces of evoked EPSCs in response to pairs of AP at 30, 50 and 150 ms intervals.

(**d**) Average paired pulse ratio in control (black, N=12) and TTX-treated (gray, N=8) connections at different inter-pulse intervals ranging from 20 ms to 250 ms. Connections in TTX-treated slices show *significant* paired pulse depression in the 50–100ms interval (**P* <0.05, ****P* <0.001, 2-way ANOVA). Error bars represent s.e.m.

(**e**) Example traces showing excitatory responses in the post-synaptic CA3 neuron evoked by repeated stimulation. Control (top) and TTX-treated (middle) slices. For a given condition in a pair of neurons, 10 traces were averaged. Bottom trace (gray) shows a 20 Hz train of five APs in the presynaptic neuron.

(**f**) Ratio of the EPSC response evoked by the fifth action potential to that evoked by the first action potential demonstrates a greatly *enhanced* short-term depression in activity deprived slices indicating an *increase* in P_r in TTX-treated slices (gray, N=6) as compared to control slices (black, N=10; **P* <0.005, unpaired two-tailed *t*-test). Error bars represent s.e.m.

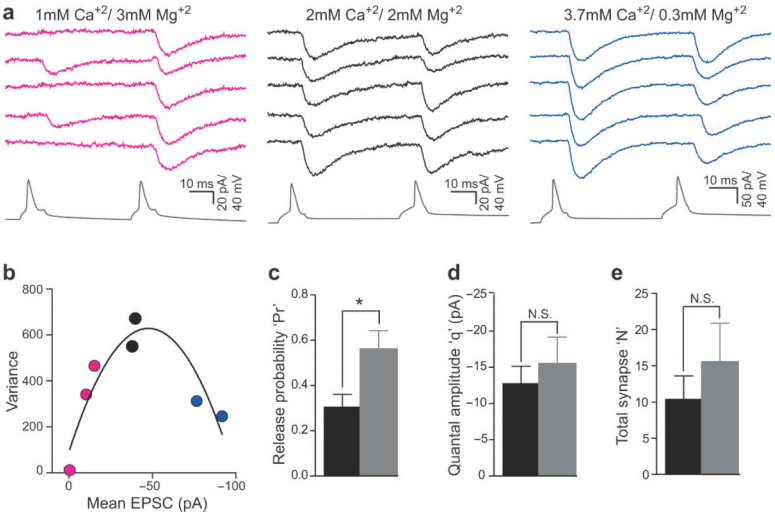

Figure 4. Variance-mean analyses

(**a**) Five consecutive traces showing responses to a pair of AP from a connected CA3 pair in three different ratios of external Ca^{+2}/Mg^{+2} concentrations (0.3, magenta; 1, black; 12.3, blue). Presynaptic AP traces shown in gray.

(**b**) Variance-mean analysis for the paired recording depicted in (**a**) plotting the variance and mean EPSC size in response to the first and second AP in three different external Ca^{+2}/Mg^{+2} concentrations and fitted with a second order polynomial (parabola).

(**c–e**) Variance-mean analysis showed a significant increase in P_r in TTX-treated slices (**c**; P <0.03, unpaired two-tailed *t*-test), but no significant change in quantal amplitude (**d**) or the total number of synapses between synaptically coupled neuron pairs (**e**). Control, black, N=11; TTX-treated, gray, N=11. Error bars represent s.e.m.

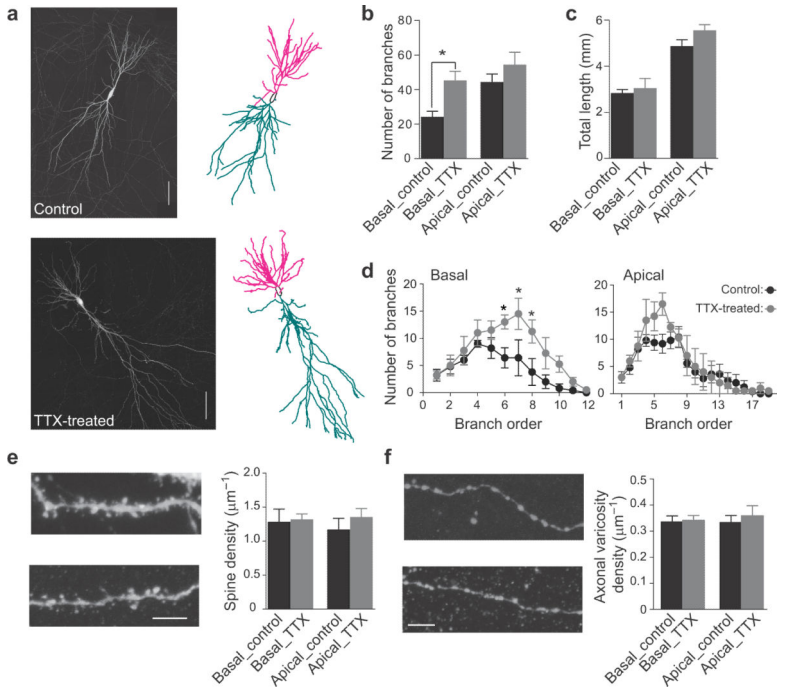

Figure 5. Morphometric change in dendrites

(**a**) Individual CA3 neurons in hippocampal slices were electroporated with EGFP at DIV 14 and imaged at DIV 24. *Left*, montage of two-dimensional z-projections of three-dimensional confocal image stacks in control (top) and TTX-treated (bottom) slices. *Right*, three-dimensional *Neurolucida* reconstruction of dendrites: basal (magenta), apical (cyan). Scale bar represents 100 μm.

(**b**) Activity-deprivation increased the average number of branches in the basal (control, black, N=5; TTX-treated, gray, N=4; $P<0.05$ unpaired two-tailed *t*-test) but not in the apical dendrites. Error bars represent s.e.m.

(**c**) Total length of basal and apical dendrites was similar in CA3 neurons from control and TTX-treated slices.

(**d**) Average number of branches for different branch orders in neurons from control and TTX-treated slices. *Left*, chronic inactivity caused an increase in branching for branch order 6–8 in the basal dendrites (control, black, N=5; TTX-treated, gray, N=4; $P<0.05$ 2-way ANOVA). No significant difference was observed for apical dendrites (right). Error bars represent s.e.m.

(**e**) Representative segment of basal dendrite from a EGFP-expressing neuron in control (top, left) and TTX-treated slice (bottom, left). Activity deprivation did not significantly change the average spine density in either basal or apical dendrites (control, black, N=5; TTX-treated, gray, N=9; right). Scale bar=10 μm.

(**f**) Example axon segment in *stratum oriens* from a CA3 neuron in control (top, left) and TTX-treated slice (bottom, left). Activity-deprivation did not significantly alter the density of axonal varicosities in the *strata oriens* or *radiatum* (control, N=5; TTX-treated, N=9; right). Scale bar=10 μm.

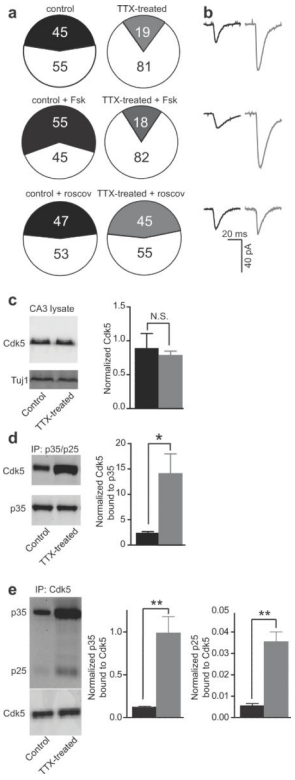

Figure 6. Activation of silent synapses

(**a**) Pie-chart depicting percentage of connected CA3 pyramids in control (black) and TTX-treated (gray) slices alone (top), after 50μM forskolin treatment (middle), and in the presence of 50μM roscovitine (bottom), respectively. Unconnected pairs, white. Numbers reflect percentages for each group.

(**b**) Average postsynaptic response from a synaptically connected neuron pair in control (black) and TTX-treated (gray) slices alone (top), after 50μM forskolin treatment (middle), and in the presence of 50 μM roscovitine (bottom), respectively; presynaptic AP not shown. Each trace represents an average of 25 sweeps.

(**c**) *Left*, western blot of CA3 tissue lysates from control and TTX-treated slices immunoblotted with the Anti-Cdk5 and Anti-Tuj1 (normalizing protein). *Right*, total Cdk5 protein levels in control (black) and TTX-treated (gray) slices were similar (control, n=42, N=4; TTX-treated, n=42, N=4; where `n' is total number of slices and `N' is number of organotypic culture batches). Error bars represent s.e.m.

(**d**) Western blot of a co- immunoprecipitation (Co-IP) assay used to identify Cdk5 physically associated with p35/p25. *Right*, activity-deprivation showed a significant increase in Cdk5 physically associated with p35/p25 (control, black; n=42, N=4; TTX-treated, gray; n=42, N=4, P<0.03, *t*-test). Error bars represent s.e.m.

(**e**) Converse Co-IP assay used to probe the amount of p35/p25 physically associated with Cdk5. Activity-deprivation showed a significant increase in both p35 (middle) and p25 (right) physically associated with CDK5 (control, black; n=42, N=4; TTX-treated, gray; n=42, N=4, P<0.01, unpaired two-tailed *t*-test). Error bars represent s.e.m.

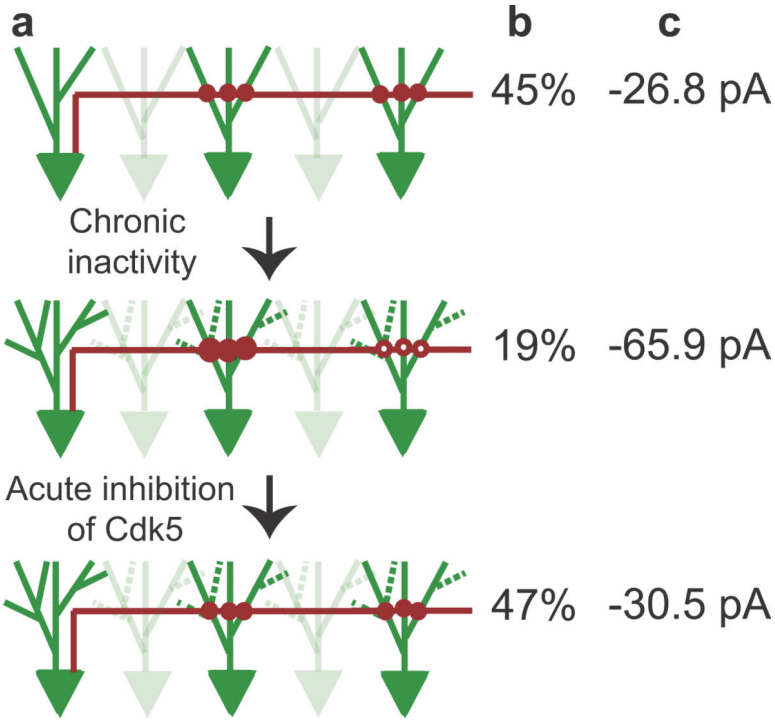

Figure 7. Model

Schematic representation of homeostatic changes in the CA3 excitatory recurrent microcircuit caused by chronic activity-deprivation and its acute reversion by CDK5 inhibition.

(**a**) In control conditions, CA3 pyramidal neurons are functionally connected to ~45% of the neighboring CA3 neurons. CA3 pyramidal cell body and basal dendrites are in green and axon in red. Filled circles denote active connections. After chronic activity-deprivation, there is a reduction in connectivity to ~20% due to presynaptic silencing of connections (empty circles). The synaptic strength of the remaining connections is increased due to a significant increase in P_r, depicted by the larger size of the red, filled circles. There is also an increase in basal dendritic branching. Acute application of roscovitine reverses the affect of chronic TTX-treatment on functional connectivity and average strength of the connections to that of control conditions.

(**b**–**c**) Average functional connectivity (**b**) and synaptic strength (**c**) of CA3 neuron pairs in slices from control, activity-deprived, and activity-deprived in the presence of roscovitine conditions.